X-ray microtomography of ice crystal formation and growth in a sponge cake during its freezing and storage

Pierre Latil, Amira Zennoune, Fatou-Toutie Ndoye, Frédéric Flin, Christian Geindreau, Hayat Benkhelifa

Journal of Food Engineering

X-ray microtomography of ice crystal formation and growth in a sponge cake during its freezing and storage

--Manuscript Draft--

Manuscript Number:	JFOODENG-D-21-00801R3
Article Type:	Research Article
Keywords:	freezing; Sponge cake; Thermal cycling; Recrystallization; X-Ray Microtomography; Image processing.
Corresponding Author:	Amira ZENNOUNE, M.D INRAE Centre Île-de-France Jouy-en-Josas Antony: Institut National de Recherche pour l'Agriculture l'Alimentation et l'Environnement Centre Ile-de-France Jouy-en-Josas Antony Antony, 92 FRANCE
First Author:	Amira ZENNOUNE, M.D
Order of Authors:	Amira ZENNOUNE, M.D
	Pierre Latil
	Fatou Toutie Ndoye
	Frederic Flin
	Christian Geindreau
	Hayat Benkhelifa
Abstract:	X-ray tomography has been used to characterize microstructural changes taking place into sponge cake upon freezing and subsequent storage at fluctuating temperatures. The CellDyM cooling cell, initially developed for snow, was used to subject a sponge cake sample to freezing and thermal cycling directly inside the X-ray tomograph. 3D images of the same sample have been scanned at different times during 6 days. An original image processing based on Digital Volumetric Correlation (DVC) has been implemented in order to segment the images and then to quantify porosity changes and ice crystal formation and growth. Overall, the obtained results have shown that (i) all the ice crystals are located at the pore surface and no crystal was found inside the sponge cake crumb matrix and (ii) during the thermal cycling, the size of the ice crystals linearly increases while the number of ice crystals tends towards a plateau. These tendencies can be related to a recrystallization phenomenon occurring due to thermal cycling. More generally, the proposed methodology could be applied to other frozen porous products during freezing and frozen storage.

Cover Letter

Amira ZENNOUNE

Refrigeration Process Engineering Research Unit
INRAE, 1 rue Pierre-Gilles de Gennes
CS 10030, 92761 Antony Cedex, France

Dear Editor,

We wish to submit a research article entitled **"X-ray microtomography of ice crystal formation and growth in a sponge cake during its freezing and storage"** to be considered for publication in Journal of Food Engineering.

In this manuscript, we report the application of an innovative X-ray microtomography–based methodology to analyze the microstructure of frozen sponge cake. The particularity of the studied product is its high porosity and its complexity which makes difficult to study and understand heat and moisture transfer phenomena. A specific cooling stage initially developed for snow was used to subject sponge cake samples to freezing and thermal cycling directly inside a laboratory X-ray microtomography apparatus. This cooling stage allows in situ monitoring of the ice crystals dynamics during freezing and frozen storage of porous foods for the first time. Dynamic X-ray microtomography generates multiple radiographs reconstructed to give the 3D volume of the sample. An original image processing based on Digital Volumetric Correlation (DVC) was implemented in order to segment the images and then quantify porosity changes as well as formation and evolution of the ice crystals.

This study brings new and strong evidences about the impact of dynamic changes of temperature during freezing and frozen storage on ice crystal characteristics (location and size) in sponge cake. Therefore, we believe that our findings could be of interest and useful for the readers of Journal of Food Engineering.

We confirm that this manuscript has not been published and is not under consideration to be submitted for publication elsewhere. All co-authors have seen and agree with the contents of the manuscript and we have no conflicts of interest to disclose.

We hereby suggest the following referees: **Gerard VAN DALEN** Gerard-van.Dalen@unilever.com **Alain Le Bail** alain.lebail@oniris-nantes.fr**.**

Thank you for your consideration of this manuscript.

Sincerely yours,

Amira ZENNOUNE

Corresponding author: Dr Fatou Toutie NDOYE at INRAE - FRISE
1 rue Pierre Gilles de Gennes, CS 10030, F-92761 Antony cedex
Tel.: + 33 1 40966161, Fax: + 33 1 40966075
E-mail : fatou-toutie.ndoye@inrae.fr

Dear editor,

Thank you for the opportunity to submit a revised version of our manuscript entitled '*X-ray microtomography of ice crystal formation and growth in a sponge cake during its freezing and storage*'. We thank the reviewer for his valuable feedback, which has contributed to the improvement of the manuscript.

Our responses to the comments below are highlighted in blue.

Reviewer #3:

The revised article contains additional supplements that would be helpful for the understanding. Additional information containing the experimental and analysis is also added and the results are compared.

Some minor concerns that the authors may want to pay attention to is:

(1) The resolution after binning is 15 micron/pixel and this is not the real resolution. The real resolution is 30-45 micron depending on conditions. So, the authors may want to modify the description related to resolution.

The initial pixel size was 7.5 micron and 15 micron after binning. Even if some image treatments such as filtering may probably modify this resolution, their effects are rarely quantified. Thus, we prefer to keep in the manuscript these values, which are commonly used and more reliable.

(2) The scale bar is better to add in the Fig. 5b.

The Figure 5b has been modified accordingly in the revised version of the manuscript.

(3) the size of scale bar should be noted in fig. 8.

The Figure 8 has been modified accordingly in the revised version of the manuscript.

Highlights

- First study of ice crystal formation and growth in a sponge cake during freezing and storage.
- In-situ freezing and thermal cycling were performed inside a laboratory X-ray μCT apparatus.
- Dynamic X-ray μCT and Digital Volumetric Correlation were implemented to quantify ice crystals.
- Ice crystals were located at the pore surface and their size increased by recrystallization due to the thermal cycling.

X-ray microtomography of ice crystal formation and growth in a sponge cake during its freezing and storage

Pierre Latil[a], Amira Zennoune[b,c], Fatou-Toutie Ndoye[b], Frederic Flin[a], Christian Geindreau[d], Hayat Benkhelifa[b,c]

[a] *Univ. Grenoble Alpes, Université de Toulouse, Météo-France, CNRS, CNRM, Centre d'Études de la Neige, Grenoble, France*
[b] *Université Paris-Saclay, INRAE, UR FRISE, F-92761, Antony, France*
[c] *Université Paris-Saclay, INRAE, AgroParisTech, 75005, Paris, France*
[d] *Université Grenoble Alpes, Grenoble INP Institute of Engineering, 3SR, CNRS, Grenoble, France*

Abstract

X-ray tomography has been used to characterize microstructural changes taking place into sponge cake upon freezing and subsequent storage at fluctuating temperatures. The CellDyM cooling cell, initially developed for snow, was used to subject a sponge cake sample to freezing and thermal cycling directly inside the X-ray tomograph. 3D images of the same sample have been scanned at different times during 6 days. An original image processing based on Digital Volumetric Correlation (DVC) has been implemented in order to segment the images and then to quantify porosity changes and ice crystal formation and growth. Overall, the obtained results have shown that (i) all the ice crystals are located at the pore surface and no crystal was found inside the sponge cake crumb matrix and (ii) during the thermal cycling, the size of the ice crystals linearly increases while the number of ice crystals tends towards a plateau. These tendencies can be related to a recrystallization phenomenon occurring due to thermal cycling. More generally, the proposed methodology could be applied to other frozen porous products during freezing and frozen storage.

1. Introduction

Freezing technologies are widely used by the pastry industry in order to preserve the products and to extend their shelf life. This is particularly the case for sponge cake, which is the base of several pastries and one of the most common frozen cake. It is usually produced in large quantities at industrial scale or in pastries following a two stage process: (i) at first, the product is baked and frozen in a factory; (ii) then, after a storage period, it is thawed, prepared and garnished just before the sale in retail stores or in artisanal pastries. This process makes it possible to produce large quantities and to distribute the product over an extended period to distant locations. However, the quality of the thawed sponge cake can be deteriorated by undesirable physico-chemical changes taking place during freezing and frozen storage, resulting in a reduction of consumer acceptance and in economic losses for the industry (Owen and Van Duyne, 1950).

It is established that these changes are closely related to ice crystals which are formed during the freezing process and which evolve during the frozen storage due to recrystallization (Le-Bail et al., 2011). In food freezing, heat transfer is always coupled with mass transfer. A temperature gradient appears between the cold surface and the core inducing a conductive heat transfer. Concomitantly, a water vapour pressure gradient between the surrounding air and the food surface occurs leading to a diffusive water transfer from the core to the surface and thus to water evaporation. During the freezing of porous foods at atmospheric pressure, this vapour diffusion is also present in the pores and is the main mass transfer mechanism (Pham, 2006). When the freezing point is reached, the liquid water is converted

into ice. Inside the pores, the supersaturated vapour also condenses into ice. This mechanism is called evapo-condensation. After freezing, ice recrystallization occurs during storage. It involves metamorphic changes of ice crystals to minimize the surface free energy of the entire crystal phase. Small ice crystals, which have a large excess of surface free energy and therefore are thermodynamically unstable tend to lower their energy level in favor of large ice crystals. The net result is the disappearance of small crystals by melting or sublimation and the growing of large crystals leading to the decrease in crystal number and the increase of the average ice crystal size. Ice recrystallization may occur according to several mechanisms such as isomass rounding, accretion or migratory (also called Ostwald ripening) (Fennema, 1973; Cook and Hartel, 2010). Among these mechanisms, Ostwald ripening which involves a melting-diffusion-refreezing process is the most prominent in frozen foods and in case of temperature cycling (Hartel, 1998; Ndoye and Alvarez, 2014; van Westen and Groot, 2018). This phenomenon that involves changes in number, size, shape and location of the ice crystals occurs at constant temperatures, but is accelerated by fluctuating temperatures that are often inevitable through the cold chain due to the on/off operation of the refrigerating equipment or to poor practices (temperature abuse) (Zaritzky, 2010).

Many efforts have been focused on the relationships between the structural quality of frozen/thawed baked products and the re-arrangement of both the starch granules and the gluten network that may be impaired by ice crystals formation and growth. Most of these studies concerned bread (Bárcenas et al., 2003; Hamdami et al., 2004; Bárcenas and Rosell, 2006; Mandala et al., 2008, 2009; Eckardt et al., 2013). A few were related to cakes (Gómez et al., 2011; Karaoğlu et al., 2008) and to sponge cake (Díaz-

Ramírez et al., 2016), the composition of which is different from that of bread and would therefore be likely to react to freezing and frozen storage differently. In opposition, the mechanisms by which ice crystals evolving at local scale interact with the development of the structure of frozen/thawed baked product are scarcely described and thus not fully elucidated. The rare studies that exist also concern bread, especially part-baked bread (Lucas et al., 2005a,b; Chen et al., 2012, 2013), but to our knowledge, no study has been carried out about sponge cake. This lack of work can be explained by the complexity of the experimental evaluation of the local dynamics of water and ice during freezing of such porous media. Nuclear magnetic resonance imaging (MRI) was used to locally assess physical changes that take place during the pre-chilling and freezing of par-baked bread (Lucas et al., 2005b). The methodology enabled to perform a continuous and non-invasive monitoring of the process, but the MRI signal was not detectable after the beginning of the crystallization. Moreover MRI signal analysis do not provide the ice crystal size and distribution. More recently, Chen et al. (2012) used differential scanning calorimetry (DSC) to investigate the effect of freezing rates on the formation and distribution of ice crystals upon the freezing of fresh breadcrumb. The authors have estimated the mean ice crystals sizes in small and large crumb pores (with sizes ranging from nanometre to millimetre) using the endotherm curve obtained by DSC and the modified Gibbs-Thomson equation. They report smaller ice crystals in small crumb pores. But both ice crystals in small and large crumb pores have sizes in the nanometer range (5 - 18 nm), far below the size of bulk ice which should be in the micrometer range or even larger. They argued that the DSC procedure (isothermal stage at -30 ^{o}C for 10 min.) used in their work did not afford enough time to make possible water migration and, consequently, the

growth of ice crystals. Indeed, the formation and growth of ice crystals are highly correlated with the water distribution and migration that may be constrained by the starch/gluten network and the crumb porosity.

From the above literature review, it is obvious that the methodologies used to characterize the dynamics of ice crystals formation and growth during freezing of porous food such as bread do not provide a satisfactory quantitative assessment. More reliable techniques are still needed to improve the understanding of the complex mechanisms taking place at this microscopic scale, particularly into such porous frozen foods. The potential of X-ray micro-computed tomography (X-ray μCT) as a reliable methodology to visualize and quantify the 3D microstructure of frozen foods with a non-destructive approach was recently showed (Vicent et al., 2017). X-ray μCT generates 3D images reconstructed from multiple radiographs acquired from different angles around a sample. X-ray μCT images reflect the sample with different grey level depending on the X-ray attenuation properties of the different components. Since commercial μCT devices are adapted for ambient temperature imaging and not equipped with thermostated stage, specific tools have been developed to maintain the samples at frozen state during imaging. Vicent et al. (2017) developed a new X-ray μCT based methodology that enables to image frozen foods at the frozen state (-20 °C), thanks to a cooling stage made with phase change material. This methodology provided valuable insights into the microstructural changes in frozen minced beef as affected by the freezing rate (Mulot et al., 2019), in frozen carrots upon storage with fluctuating temperature (Vicent et al., 2019) and in fresh ice sorbet after freezing (Masselot et al., 2021). However, the cooling stage used in these works does not allow analysing the frozen sample more than 20 minutes, thus making in-situ monitoring of the water/ice crystals dy-

namics during an extended period impossible. Moreover, it does not allow dynamic monitoring of temperature in order to perform thermal cycling that may mimic temperature fluctuations occurring through the cold chain. Guo et al. (2018) successfully applied in situ synchrotron X-ray μCT to investigate dynamic microstructural changes of ice cream subjected to thermal cycling, using a cooling stage specially designed to operate between ambient temperatures to -40 °C. A similar cooling stage was used by Calonne et al. (2015) in a laboratory scale X-ray μCT apparatus to dynamically monitor the metamorphism of snow. The advantage of this cooling stage, named Cell for Dynamic Monitoring (CellDyM), is to allow precise setting of the temperature at the top and the bottom of the sample using Peltier coolers. An aluminium sample holder was used allowing a vertical heat conduction and a subsequent uniform temperature within the sample. But all overmentioned studies concerned non porous foods or systems containing a high water fraction and with ice crystals already formed. In the specific case of sponge cake, the water content is low and is trapped in a porous starch/gluten matrix. Following the formation and growth of ice crystals, as well as the evolution of pore structure into such a complex microstructure is really challenging.

The principal purpose of the present study was to apply a dynamic X-ray μCT based methodology to assess the local physical changes taking place into sponge cake upon freezing and subsequent storage at fluctuating temperatures. To this end, the CellDyM cooling stage developed by Calonne et al. (2015) for snow was used to subject sponge cake samples to freezing and thermal cycling directly inside the X-ray μCT apparatus. Scans were performed at different times during 6 days-period of analysis. An image analysis strategy based on Digital Volumetric Correlation (DVC) (Buljac et al., 2018) was implemented to quantify porosity changes and ice crystals

formation and evolution. Cryo-SEM analysis was also perfomed to obtain high resolution imaging and to qualitatively compare the microstructure obtained with cryo-SEM and μCT image visualization.

2. Material and methods

A specific sponge cake formulation and preparation protocol was defined and optimized (see section 2.1) to ensure reproducible cakes in terms of thermophysical properties (density, water content and freezing point) (see section 2.2).

2.1. Sponge cake preparation and sampling

Sponge cakes were home made using the following formulation: 25 % (w/w) wheat flour (farine de blé, Tarwebloem T55, Germany) , 25 % (w/w) sucrose (powdered sugar, Daddy, France), and eggs (Carrefour Bio, France): 30 % (w/w) egg white, 15 % (w/w) egg yolk, and 5% (w/w) of pure water. These ingredients were purchased from local supermarket.

The batter was prepared using a kitchen food processor (Masterchef Gourmet QA510110, Moulinex, France) into two steps:

1. First, egg yolk was homogenized for 10 s, then sugar was incorporated and blended for 10 min 12 s , afterwards sifted white flour was gradually poured over 2 min 12 s and finally water was added and blended for 1 min. All these blending operations were performed at maximal speed rotation of the kitchen food processor. The mixture is then left;
2. Egg whites got beaten separately using the same food processor at high speed. Finally, the beaten egg whites were gradually incorporated into the first mixture using a flat beater at low speed. Next, a batch of nine pieces of sponge cake was prepared by pouring 60 g of batter in each

rectangular aluminium pan (10×6×3 cm) and baked in an electrical oven (Arianna LED Bakerlux, Unox) for 20 minutes at 170 °C.

After baking, the nine sponge cakes were allowed to cool at ambient temperature for 45 minutes (ambient relative humidity RH=50-60%). They were then individually packaged in impermeable plastic bags and sealed before storage in a fridge at 5 °C (for about 7-10 days). In order to make sure that all samples have similar thermal history during baking and cooling, preliminary tests were performed using temperature sensors to record cakes temperatures. Among the nine sponge cakes prepared for this study, eight were used for DSC, density and water content measurements. According to the reproducibility of these measurements on the sponge cakes (see section 2.2), it was reasonably assumed that the latter one, which was used for X-ray tomography analysis, presents similar properties.

For X-ray μCT analysis, a sample (diameter = 9.8 mm and height = 10 mm) was extracted from the cake crumb in a cold room (-5 °C, RH=20 %) using a core drill mounted on a milling machine. The sample was transported in a sealed container at -5 °C before its installation in the cooling stage CellDyM, which ensures the needed thermo-hygroscopic stability (Figure 2).

2.2. Characterization of thermo-physical properties of the sponge cake

2.2.1. DSC measurements

The freezing point and the freezable water content were calculated using differential scanning calorimeter (DSC 1 STARe System, Mettler-Toledo, Columbus, USA). The heat flows and temperature were measured on three replicates with an accuracy of 0.02 μW and 0.02 °C respectively. For each analysis, a sponge cake sample of approximately 9 mg was placed in an

aluminium pan and hermetically sealed. For each scan, the sample was first equilibrated at 25 °C for 10 min, then cooled to -40 °C at 10 °C/min, then after an isothermal holding stage at -40 °C for 10 min, the sample was heated back to 25 °C at 5 °C/min. The onset temperature (T_o) and the peak temperature (T_p) were determined from the endothermic ice melting peak using the STARe Evaluation software (Mettler-Toledo, Columbus, USA). T_o represents the freezing point. It is defined as the intersection point between the baseline and the inflexion tangent at the beginning of the melting peak. A typical thermogram of melting is shown in Figure 1). It shows that ice melting started when the temperature reached -30 °C ; the endothermic ice melting peak was obtained at around -10 °C.

T_o measured from the ice melting endotherm was about -21 °C for sponge cake samples. Based on these DSC results, the thermal cycling during the microtomographic analysis was set between -30 °C and -20 °C , corresponding to the temperature range of the phase change into the sponge cake. This temperature range mimics the thermal fluctuations encountered during frozen storage.

2.2.2. Density

The theoretical density of batter (in kg/m^3) was first determined by considering the proportions and densities of each ingredient. The density of wheat flour, sucrose, egg white and egg yolk were measured by weighing (Mettler AE 163, precision 10^{-4} g) 10 mL of each ingredient using a measuring cylinder (three replicates). The theoretical density of batter obtained was then 941 $\pm$3 kg/m^3. Then, the density of batter was measured by weighing 100 mL of batter (two replicates) in a measuring cylinder. The measured average density of batter was equal to 700 $\pm$ 2 kg/m^3. In fact, air

was incorporated in the batter during whipping explaining this lower value of density.

The apparent density of the sponge cake was calculated by weighing (about 19 g) a parallelepiped-shaped (5.5×5.1×2.5 cm^3) sample previously cut in the sponge cake crumb. Four replicates were measured. In order to determine the density of the sponge cake without air (real density), the same samples were compacted using a vacuum sealing system (Foodsaver, V2860) to remove the air from the pores, before measuring the new dimensions for calculating the new volume. The mean apparent density and the real density of sponge cake were equal to 405 ±18 kg/m^3 and 684 ± 29 kg/m^3 respectively. The real density is close to the density of batter (700 ± 2 kg/m^3) but lower than the theoretical density of batter (941 ± 3 kg/m^3). Even after compaction, a fraction of air seems to be still present and trapped in the cake. The amount of air present inside the sponge cake was then calculated considering the ratio between the apparent density (405 ± 18 kg/m^3) and the batter theoretical density (941 ± 3 kg/m^3). The value of the mean porosity of the sponge cake equals 57 ± 2 %.

2.2.3. Water content

Five samples (6×5.8×2.2 cm^3) from different sponge cakes were cut and weighed (about 24 g). Then the water content of the samples was determined by weighing (Mettler AE 163, precision 10−4 g) before and after complete dehydration in an oven (Themarks TS4057) set at 105 °C for 24 hours. Water content is calculated as follow:

$$X_w = \frac{m_0 - m_f}{m_0} * 100 \quad (1)$$

where X_w is the water content of the sponge cake sample, m_0 is the mass (kg) of the wet sample and m_f is the mass (kg) of the dried sample. The

247 average water content was calculated from five replicates and was equal to
248 30.50 ± 1.7 %.

249 *2.3. Cryo-SEM Analysis*

250 Cryo-SEM measurements were carried out in an external laboratory
251 equipped with scanning electron microscopy (Electron Microscopy Facility,
252 IBPS, Paris, France), in order to compare imaging results to those obtained
253 with the microtomographic method. Both previously frozen and unfrozen
254 samples were analyzed. Fracture was performed in liquid nitrogen. Frac-
255 tured surfaces were observed using cryo-SEM (GeminiSEM 500, Zeiss) at
256 -120 °C, the pressure in the equipment was 1.6×10^{-4} Pa. The accelerating
257 voltage was 3.00 kV or 0.790 kV and the accessible magnification range was
258 from x13 to x500 000. Frozen samples were first observed at -120 °C then
259 after partial sublimation at -90 °C for 1 min.

260 *2.4. In situ X-ray micro-tomography*

261 *2.4.1. Cryogenic cell*

262 CellDyM is a cryogenic cell that allows the sample to be monitored
263 by time-lapse X-ray μCT with a scanner operating at room temperature
264 (Calonne et al., 2015). The geometrical arrangement of the cell enables a
265 360° rotation during a tomographic acquisition (Figure 2). CellDyM gives
266 the possibility to precisely impose the temperature (about +40 to -40 °C)
267 at the top and bottom of the sample (minimal thermal gradient lower than
268 3 °C/m) with copper cylinders while its lateral sides are thermally insulated
269 from the outside using a vacuum chamber. The sample holder mechanically
270 links the two copper cylinders and is in contact with the lateral sides of the
271 sample. This key part can be made of poly methyl methacrylate (PMMA),
272 whose advantage is to have low X-ray linear absorption and then maximise

the images contrast of low X-rays absorption samples. However, it has the drawbacks not to fully prevent from thermal radiative exchange with the outside and it is not a good thermal conductor. Alternatively, it can be made of aluminium, which allows a rather good thermal conductivity with the top and bottom copper cylinders and prevents thermal radiative transfers. In this case, the higher linear X-ray attenuation impinges the contrast within the sponge cake sample. After some trials, the aluminium sample holder appeared as the best compromise for this experiment.

2.4.2. Freezing and thermal cycling

Figure 3 shows the temperature applied to the sample with respect to the time, where the dots represent when the X-ray μCT scans (noted Si) were performed. The scans were acquired at least 30 minutes after the thermal loading to prevent the blurring of the 3D images due to the induced sample movement during acquisition. Then, after two scans (S0 and S1) in the initial state at 5 ^{o}C , the sample was frozen at -30 ^{o}C with a cooling rate of about -5 ^{o}C min^{-1} (S2). It was then warmed up at -20 ^{o}C and cooled at -30 ^{o}C 7 times at the same temperature rate (+ or - 5 ^{o}C min^{-1}). These values were measured at the cooling modules and not directly within the sample, consequently the temperatures and the cooling rate may be slightly lower. These temperature oscillations were simulating the possible temperature fluctuation during frozen food handling and storage. The whole experiment took about 6 days and all the 37 scans, hereafter noted Si with i $\in [0, 37]$, were not equally spaced in time (Figure 3) due to experimental and practical reasons.

2.4.3. 3D image acquisition

The sample was placed in CellDyM cell, which was previously installed in the tomograph cabin (RX Solutions, France) and the temperature was set to 5 °C. The system was operating at a X-ray tube voltage of 65 kV and a current intensity of 115 µA. A voxel size of 7.5 µm was set according to the dimensions of the cryogenic cell (Figure 2). The total scanning time was set at 2 hours 10 min (1440 radiographies on a 360° rotation) for one acquisition. These parameters were chosen as the best compromise between image quality (air/ice/cake contrast) and scan duration that prevents possible sample evolution during the acquisition. XAct 2 software (RX Solutions, France) was used to reconstruct the 3D volumes using the classical filtered back-projection algorithm and applying ring artefact filter.

2.4.4. Image processing

The 3D image processing involved several operations summarised in Figure 4:

Registration. All the 3D images (i.e. 37 in total), were registered in order to define and follow the same volume of analysis inside the aluminium sample holder between the two copper cylinders (Figure 5 (a)). The registration was done by setting vertical the axis of the aluminium cylinder.

Crop. All the 3D images (i.e. 37 in total), were cropped to exclude the copper cylinders absorption artefacts (Figure 5 (a)). Consequently, the height and the volume of the analyzed sample were $H = 7.9$ mm and $V_0 = 593$ mm^3.

Binning. A 2×2×2 binning was applied to all the 3D images leading to a voxel size of 15 µm and reducing the overall number of voxels by 8 to optimize

subsequent images processing, such as the digital volume correlation step.

Air segmentation. The air phase was segmented using a global grey level threshold. As shown by the grey levels histogram (Figure 5 (c)), the segmentation of air, matrix and ice was not trivial. However, the grey levels of the air phase are fairly well described by a Gaussian distribution and are expected to be constant during the experiment (no density change). The grey level threshold was chosen such that, statistically, the major part of the voxels belonging to the air phase are selected. It corresponds to the right part of the Gaussian curve fitted on the air grey levels (Figure 5 (c)). If the cake matrix grey levels are described by a Gaussian distribution, the total grey level histogram still exhibits a non negligible number of voxels with intermediate grey levels. These voxels can at least be related to both the ice crystals (Figure 5 (b)) and the partial volume effects of the matrix, *i.e.* the voxel that are at the interface of the cake matrix and the air have intermediate grey levels which is a well known artefact (Glover and Pelc, 1980). Even if it was possible to visually distinguish the ice crystals, an acceptable segmentation was not achievable for two reasons: (i) the poor grey level contrast between the matrix and ice, and (ii) some similar morphological characteristics of the ice and matrix (small and narrow). Subsequently, Digital Volumetric Correlation (DVC) has been implemented to detect the ice crystals in the 3D images.

Digital Volume Correlation (DVC). This technique is widely used in mechanics of materials to measure the deformations of a sample that has been mechanically loaded (Lenoir et al., 2007; Roux et al., 2008; Hild et al., 2011; Pierron et al., 2013), but also to detect cracks (Limodin et al., 2011; Leplay et al., 2013; Wang et al., 2016). According to Buljac et al. (2018), the

principle of DVC is the following: suppose two 3D images denoted as $f(\mathbf{x})$ (assumed to be the *reference* image) and $g(\mathbf{x})$ (the *deformed* image), where f and g are the grey levels at each voxel location $\mathbf{x}$. For the two 3D images to be correlated, DVC rests on the basic assumption that upon a mere change in the position of voxels, defined by a displacement field $\mathbf{u}(\mathbf{x})$, the two images can be brought to perfect coincidence such that $g(\mathbf{x} + \mathbf{u}(\mathbf{x})) = f(\mathbf{x})$. Although this equation appears trivial at first glance, its resolution is not, and presents a number of common issues discussed in Buljac et al. (2018). In the present work, the YaDICs software (Seghir et al., 2014) with a Finite Element Regularized DVC method was used to correlate the 3D images acquired during the experiment.

In the following, the S3 image (at -30°C) was used as the reference 3D image and was then correlated to the other 3D images (S4 to S36). It was not possible to use S0, S1, and S2 as reference images for two reasons: (i) the sample deformation between S1 (or S0) and S2, *i.e.* when the sample was frozen (Figure 3), was too important and thus DVC did not work, and (ii) the S2 image was a bit blurred due to sample evolution during the acquisition.

Ice segmentation. Besides the three components of the displacement vector $\mathbf{u}(\mathbf{x})$, the software provides the residual map of the correlation $r(\mathbf{x}) = g(\mathbf{x}) - f(\mathbf{x})$ (Figure 5 (d)). On this residual map, a grey level $r(\mathbf{x}) = 0$ indicates that the correlation is perfect, a grey level $r(\mathbf{x}) > 0$ represents a part of the image that has disappeared, *e.g.* bright voxels that became darker like when a crack occurs. Lastly, a grey level $r(\mathbf{x}) < 0$ represents a part of the image that has appeared, *i.e.* dark voxels that became brighter, or in the present case, when ice crystals appear in pores of the matrix. The obtained residual

maps mainly exhibits a good average correlation between the images with

$$\langle r(\mathbf{x}) \rangle = 1/V \int r(\mathbf{x}) dV \approx 0 \tag{2}$$

as shown by the grey level histogram plotted in Figure 5 (f). Ice crystals are clearly visible on the 3D residual maps (in black in Figure 5 (d) and (e)) and in the histogram (Figure 5 (f)) represented with grey values below -10.0. Indeed, the offset between the Gaussian fit that models the correlation residue of the random noise (which is function of the acquisition, the image's reconstruction and the data processing), and the $r(\mathbf{x})$ data highlights that objects have appeared during the experiment. Consequently, the obtained 3D residue images have been used to segment the ice phase using a global grey level threshold. The threshold level was set such that no voxel belonging to the correlation error is taken into the ice phase. The ice phase was thus segmented as all the voxels with grey values lower than -10.0 (Figure 5 (f)) and errors were estimated using two more threshold values (-12.0 and -9.0).

Matrix segmentation. The matrix (cake) phase was segmented as the remaining volume.

This image processing leads to 3D images where the 3 phases of the sample are labelled, *i.e.* 3D images with artificial grey levels that represent each phase, here $f(\mathbf{x}) = 0$ outside the region of interest (ROI), $f(\mathbf{x}) = 1$ for air, $f(\mathbf{x}) = 2$ for ice and $f(\mathbf{x}) = 3$ for the remaining voxels that belong to the matrix phase (respectively in white for air, yellow for matrix and blue for ice in Figure 5 (g) and (h)).

2.4.5. Microstructural parameters

Several microstructural parameters have been computed from the 3D labelled images in order to characterize the evolution of the microstructure induced by the thermal loading:

Porosity / ice volume fraction / matrix volume fraction. These three parameters were computed using a standard voxel counting algorithm. The porosity, the ice volume fraction, the matrix volume fraction are defined as V_{air}/V_0, V_{ice}/V_0 and V_{matrix}/V_0 respectively, where V_{air}, V_{ice} and V_{matrix} are the volume of each phase and V_0 is the initial volume of the sample (Figure 6). All these quantities are computed using the initial volume of the sample V_0 as reference (Lagrangian quantities). As will be shown later, the sample volumes change during the experiment due to the matrix shrinkage (Section 3.4), so the current volume of the sample is smaller than the initial one.

Specific surface areas. The surface areas of the interfaces, $S_{\text{matrix/air}}$, $S_{\text{ice/matrix}}$, $S_{\text{ice/air}}$ have been computed using the MorphoLibJ tools (Legland et al., 2016) on the labelled 3D images. It was then possible to estimate the corresponding Specific Surface Areas (SSA) defined as SSA = $S(\text{interface})/V_0$ (Figure 6) and expressed in mm^{-1}.

Ice crystals and pore granulometry. Using a typical connected component analysis, performed with the MorphoLibJ library (Legland et al., 2016), it was possible to compute the granulometry of the ice crystals, *i.e.* to count the ice crystals N^{ice} in the 3D image and to compute their characteristic dimension defined here as the equivalent diameter of an ice crystal (the diameter of a sphere with the same volume as the particle):

$$d_{\text{eq}}^{\text{ice}} = 2\sqrt[3]{(3/4\pi)V^{\text{ice}}}, \tag{3}$$

with V^{ice} its volume. According to the resolution after the binning operation, the critical size of the ice crystals which can be measured is 15 µm. It

was also possible to compute the pore granulometry. Even if the pores are connected, the porous network was artificially divided into individual pores using the 3D watershed algorithm of the MorphoLibJ library (Legland et al., 2016). An additional borderkill algorithm (Legland et al., 2016) was applied to remove the pores in contact with the aluminium sample holder. Then, as for the ice crystals, it was possible to count the number of pores N^{pore} and to compute their equivalent diameter $d_{\text{eq}}^{\text{pore}}$.

3. Results and discussion

3.1. Microstructural observations

Cryo-SEM was used to visualize the microstructure of model sponge cake after freezing. Figure 7 shows a micrographs of a frozen sample at magnification of x500. The formation of ice crystals can be observed; they are partially embedded into the wall and protrude into the pores. The typical size of such crystals is about 20 µm. Even if there are few crystals which are a little bit smaller, the used resolution for the X-Ray 3D images after binning (15 µm) is sufficient to capture most of the crystals.

Figure 8 presents vertical slices of some 3D images acquired during the experiment. The global evolution of the sample can be observed, as well as the local one through the insets in the surroundings of a pore of characteristic dimensions of 1.2×0.8 mm^2. The sponge cake exhibits a highly porous microstructure: (i) the air volume fraction is about 79 % and (ii) the connected pore network presents a large variety of pore sizes. This mean porosity is higher than the one initially determined by density measurements (57%) and described in section 2.2.2. These differences can be mainly explained by the heterogeneity of the sponge cake, the presence of large pores

and the volume of the sample that was nearly 80 times higher in the case of density measurements.

Overall, the sample seems not to undergo many modifications during the experiment, except at the beginning during the freezing stage. Indeed, from S0 (T=5 °C, t=0 h) and S3 (T=-30 °C, t=8.8 h), an important shrinkage of the sample can be observed as shown by the black arrows on the S3 slice (Figure 8). In the initial state S0, the sample is in contact with the aluminium sample holder (Figure 8) while in S3 there is an average air gap of 0.25 mm between the aluminium holder and the sample. Then, this gap sligthly decreases during each warming-up. At the end of the experiment (S36), this gap is at an average of around 0.3 mm.

At the pore scale, small crystals (of about 50 μm or less) mainly appear and grow at the matrix-air interface (red arrows in Figure 8), which is consistent with Cryo-SEM observations (Figure 7). These particles have a grey level intensity, *i.e.* a linear X-ray attenuation coefficient below the one of the matrix (about 10% less). The number and the size of these crystals depend on the freezing time and the temperature. During the warming-up stage, some ice crystals can totally or partiallly disappear (see red arrows in S18-S22 and S27-S31, Figure 8).

3.2. Porosity and pore sizes

As already mentionned, the sponge cake sample exhibit a highly porous microstructure and about 99% of the air volume was found to be connected, *i.e.* the volume of pores trapped in the matrix was less than 1% of the total air volume in the sample.

The pores size and distribution computed from the 3D images are presented in Figure 9. Figure 9 (a) shows that most of the pores are within

the range 0.1 to 0.9 mm. The number of pores with $d_{\mathrm{eq}}^{\mathrm{pore}} < 0.4$ mm slightly decreases during the experiment. No pore with $d_{\mathrm{eq}}^{\mathrm{pore}} < 0.1$ mm is detected for the S36 scan. This can be explained by the shrinkage of the sample that decreases the pores size and makes the smallest ones not detectable by the experimental set-up. This is not an image processing artefact since $d_{\mathrm{eq}}^{\mathrm{pore}} = 0.1$ mm is much larger than the image voxel size (0.015 mm). On the other hand, the characterization of the largest pores (typically with $d_{\mathrm{eq}}^{\mathrm{pore}} > 1.0$ mm) may undergo some image processing issues. Some of the biggest pores might be over-splitted while others are under-splitted by the 3D watershed algorithm. Despite such image processing issues, the 3D images clearly show that the sponge cake matrix presents some large pores whose diameters are within the range $1 - 5$ mm.

The number of pores is initially about 5000 (Figure 9 (b)), and their mean equivalent diameter is about 0.4 mm (Figure 9 (c)). During the experiment, the number of pores decreases while the mean equivalent diameter increase. These evolutions are mainly related to the shrinkage of the matrix during the experiment. Indeed, as already underlined, due to the shrinkage, the smallest pores with a diameter below 0.1 mm may disappear or become too small to be detectable. Consequently, the number of pores decreases and the mean equivalent pore size increases.

3.3. Sample shrinkage

Figure 10 presents the evolution of sample volume during the experiment divided by its initial volume. The shaded area represents the estimated errors obtained with different grey level thresholds (see Section 2.4.4). This figure shows that during the first freezing stage (from S0 (T=5 ^{o}C, t=0 h) to S3 (T=-30 ^{o}C, t=8.8 h), the shrinkage of the sample is about 4%.

After 32 hours at -30 °C (S11), this shrinkage attains nearly 6%. During the seven warming-up/cooling cycles, this shrinkage is almost stable and oscillates between 5% and 8%. The shrinkage phenomena is discussed in the section 3.7.3.

3.4. Evolution of the volume fraction of each phase

The vertical profiles of the 3 phases' volume fractions are plotted in Figure 11. These profiles show that the vertical distribution of the three phases is not perfectly homogeneous. The variations are typically around 10% for the matrix and air volume fractions (Figure 11 (a) and (b)). Despite such heterogeneities, Figure 11 shows that the shape of these profiles are quite similar during the experiment, indicating an homogeneous phenomenon along the height of the sample. On the other hand, the ice volume fraction profiles plotted in Figure 11 (c) show that the ice content increases during the experiment and that this phenomenon is also rather homogeneous in the sample.

Figure 12 shows the evolution of the volume fractions of the 3 phases during the whole experiment. Both matrix and air volume fraction are mainly decreasing, respectively at a rate of -8.5 10^{-5} h^{-1} and -8.6 10^{-5} h^{-1}, as shown by the linear regressions plotted on Figure 12 (a) and (b). By contrast, the volume fraction of ice increases and reaches a final value of about 0.024 ± 0.006 at the end of the experiment. All these evolutions are mainly related to the shrinkage process and the crystals growth. During the freezing stage, the water initially present in small pores of the matrix has migrated in the larger pores network and then has been transformed in ice crystals. This leads to a decrease of the volume of the matrix, but also of the volume of the pores due to both the disappearance of the smallest pores

within the matrix and the crystals growth within the large pores.

Finally, the ice volume fraction was computed and presented in Figure 12 (c). Using S3 scan as a reference, this measurement does not take into account the ice initially present in S3 due to the freezing. However, the Figure 12 (c) shows that after 8 hours (S4), the ice volume fraction is very low and is about 0.02%. As a consequence, it seems reasonable to suppose that the ice volume fraction that might be present in the reference scan S3, made 2 hours after freezing might be as low as 0.005%. Consequently, the error that was made by considering the S3 scan as a reference is negligible.

3.5. Ice crystals properties

Figure 13 presents 3D rendering of the sponge cake after segmentation at different time of the experiment. Within the chosen 3D images, the first ice crystals (in blue) are visible for S11. They cover the matrix surface fairly evenly with maybe a preference for narrow regions (small pores), and are small (characteristic dimensions of $20 - 25$ µm) with round shapes.

During the thermal cycle, the number of ice crystals increases. They present different shapes and dimensions, ranging from small rounded particles to angular shaped crystals with a length of 0.1 mm and an aspect-ratio between 3 and 4. During the warm-ups, the ice crystals size decreases globally. Consequently, some of the smallest crystals can disappear and the number of crystals thus decreases. However it seems that some large crystals are not affected, their size remain almost constant and even grow (see S27-S31 in Figure 13).

The distribution of the ice crystals equivalent diameter $d_{\text{eq}}^{\text{ice}}$ is plotted in Figure 14 (a). This figure shows that in the early stage of the experiment, about 80% of the total ice volume is composed of ice crystals such as $d_{\text{eq}}^{\text{ice}} < 30$

µm. By contrast, in the last steps of the experiment, more than 95% of the total ice volume is composed of particles with size higher than 30 µm. The maximum equivalent diameter measured is about 150 µm.

Figures 14 (b) and (c) show that the total number of ice crystals N^{ice} strongly increased up to 350,000 and that the mean ice crystal volume $\langle v^{\text{ice}} \rangle$ increased linearly up to 40,000 μm^3. It must be mentioned that during the first steps after the freezing, the granulometry of the ice crystals is less accurate due to the resolution of images and the precision of the image processing, *i.e.*, the smallest particles may not be detected or with a low precision. Finally, as already mentioned, the number of ice crystals decreases of about $15-20\%$ after each warm-up cycle and the size of the crystals also decreases.

3.6. Specific surface areas

Figure 15 presents the evolution of the three SSAs: $\text{SSA}_{\text{matrix/air}}$, $\text{SSA}_{\text{ice/air}}$ and $\text{SSA}_{\text{ice/matrix}}$. We can observe that $\text{SSA}_{\text{matrix/air}}$ is about 10 mm^{-1} at the beginning and slightly decreases during the experiment. This decrease is linked to the apparition of the ice crystals mainly at the interface air-matrix. Consequently, the $\text{SSA}_{\text{ice/matrix}}$ increases and tends towards 1 mm^{-1} at the end of the experiment, i.e. around 10% of the air-matrix interface is covered by ice crystals.

Finally, the differences between the SSA values of the two first scans S0 and S1 are very small. While their acquisition time was separated by 3 hours, these results show: (i) the stability of the sample in the experimental set-up, and (ii) the ability of the image analysis to provide repeatable data.

3.7. Discussion - Physical processes

3.7.1. Ice crystals location

One specificity of applying X-ray μCT to follow ice crystals formation and growth is the possibility to get a mapping of ice crystals into the frozen sponge cake crumb. Figures 5 (g) and (h) give a 2D representation of this ice crystals mapping. A 3D rendering is shown in Figure 13. In both renderings, ice crystals labelled in blue seem to be located essentially at the matrix-air interface. This observation is more precisely demonstrated in a schematic representation at local scale (Figure 6). All ice crystals are found to surround partially the pores surface and no crystal was located inside the sponge cake crumb matrix. Furthermore, the SSA evolution of ice shown in Figure 15, points out that the ice-air interface is always larger than the ice-matrix interface. Moreover, the SSA of matrix with air decreases inversely with the increase of SSA of ice with air. But SSA of the matrix with air and ice remains constant over time. This result also supports the hypothesis that ice crystals are mainly formed at the periphery of the pores and grow inside the pores. Similar conclusion were reported by Chen et al. (2012) who studied ice crystals formation and distribution in wheat bread, using DSC measurements. The DSC thermograms obtained in their study show a minor ice melting endotherm that precedes a major one. The authors attributed the minor endotherm to the melting of ice crystals located in tiny pores and capillaries within the gluten-starch matrix. In contrast, the major endotherm would be due to the melting of large ice crystals housed in gas cells that form large pores. It is worth noting that the smallest pore and ice crystal size observable in our study corresponds to the image voxel size (15 μm). Nevertheless, it is quite possible that even smaller pores are embedded inside the matrix and that ice crystals have formed and grown

inside without reaching a size detectable with the method used in this study. Other authors also argued that ice crystals formed upon freezing of porous food materials are mainly originated from pores (Baier-Schenk et al., 2005; Kontogiorgos and Goff, 2006; Kontogiorgos et al., 2008). Baier-Schenk et al. (2005) imaged ice formation during freezing of bread dough and observed first ice crystals formation at the pore interfaces. They concluded that gas pore interfaces are preferential sites for ice nucleation thus favouring the growth of ice crystals into the pores. They also admitted that small ice crystals formed inside the dough matrix but are of smaller size than the ice crystals inside the gas pores. The random nature of nucleation makes it difficult to know the exact mechanisms involved on the surface of the pores. But, the structured aspect of pores surface may promote the nucleation because of irregularities that can constitute nucleation sites (Baier-Schenk et al., 2005). There is no consensus about the mechanism by which ice nucleation occurs at the pores surface. The most plausible mechanism would be related to the coupled heat and moisture transfers that take place during freezing of porous foods and known as evapo-condensation phenomena. This theoretical model has been found to correctly predict the large variations of thermophysical properties with temperature in porous foods (Hamdami et al., 2004). In the case of sponge cake, when the product temperature is cooled down, the matrix phase becomes warmer than the pores. Indeed, the thermal diffusivity of the air inside the pores is much higher (nearly 10^{-5} m^2/s) than the sponge cake matrix thermal diffusivity (around 10^{-8} m^2/s). Water thus diffuses through the matrix and evaporates inside the pores. Once the pores surface reaches the freezing point, the water vapour inside the pores condenses at the pores surface, thus initiating ice formation.

3.7.2. Ice crystals growth and recrystallization

In-situ X-ray µCT allows us to follow the ice crystals profile into the same frozen sponge cake crumb during thermal cycling (-30 °C to -20 °C) over a period of 6 days. Ice crystals size distributions over time are depicted on Figure 14(a). It can be seen that the distributions are shifted to the right side when aging time rises, showing an increase of ice crystals size with time. First observable ice crystals were detected for S4 (about 18h at -30 °C) with sizes ranging from 15 to 50 µm and 80% of the particles with sizes smaller than 30 µm. For S11 (about 41h at -30 °C) which is the last scan before the beginning of the thermal cycling, the ice crystals size distribution slightly enlarged to a maximum size of 60 µm, but 70% of particles are still very small with sizes lower than 30 µm. This result shows a very low growth of ice crystals between S4 and S11. On the other hand, the number of ice crystals increased 10 times during this period at -30°C as can be seen on Figure 14(b). The present result may be related to the fast freezing rate (15 °C min^{-1}) that implies a high super-cooling leading to the formation of numerous ice nuclei with small critical size for growth. Furthermore, the fast freezing rate combined to the low temperature slows down water diffusion resulting on limited growth of nuclei and small ice crystals. The increase in ice crystals number could be explained assuming two mechanisms that happen concomitantly (Figure 16): (i) nucleation continues and new ice crystals are formed, (ii) existing ice crystals grow from local freezable water in the surrounding space to reach an observable size. From S12 to S36 (the last scan), ice crystals size distributions continue to expand steadily reaching a maximum size of 150 μm as shown in Figure 14(a). During thermal cycling, the mean ice crystal volume exhibits a quasi-linear increase (Figure 14(c))

while the increase of the number of ice crystals is strongly slowed down and seems to tend towards a plateau (Figure 14(b)). Temperature cycling near the melting point of ice in the sponge cake crumb (-21 °C) increased water mobility and promotes further growth of ice crystals by recrystallization phenomenon based on Ostwald ripening. In the case of porous foods, recrystallization by Ostwald ripening may involve both melting-diffusion-refreezing or sublimation-diffusion-condensation processes (Zariztky, 2008). Indeed, the DSC thermogram displayed in Figure 1 shows the co-existence of ice and liquid water (from melted ice) within the thermal cycling temperature range (-30 °C / -20 °C). Depending on the temperature and pressure local conditions within the product, melting or sublimation of ice can occur. When the sponge cake is warmed up, small ice crystals, which have a low energy stability, tend to melt/sublime and can even completely disappear. Water molecules thus released are redistributed through the sample and are redeposited onto large ice crystals, which are thermodynamically favoured. As mentioned earlier, in the case of porous materials, water redistribution occurs preferentially towards the pores where large ice crystals get bigger. Both melting-diffusion-refreezing and sublimation-diffusion-condensation mechanisms yield to a decrease of ice crystals number and to larger ice crystals size in the sponge cake. The fact that the number of ice crystals does not effectively diminish in this study might be explained by the continuous growth of small ice crystals, which become more and more detectable as the thermal cycling progresses. These results are in line with the findings of Chen et al. (2013) who reported ice crystals growth by recrystallization during aging of frozen wheat bread, eventhough they do not measure ice crystals size directly. Bárcenas and Rosell (2006) also reported similar results for long-term storage of frozen par-baked bread without evidencing the ice crystals

growth by direct measurements. Recrystallization was also found to be responsible for ice crystals growth and consequent microstructure destruction during aging of frozen flour-water mixture using nuclear magnetic resonance and transmission electron microscopy (Kontogiorgos and Goff, 2006). But, to our knowledge, there is no published work describing *in situ* ice crystals formation and growth while quantifying ice crystals size in frozen sponge cake.

3.7.3. Skrinking behaviour

Sponge cake shrinkage of about 4-6 % was observed at the early stage of the freezing process when the product temperature passes from 5 °C to -30 °C (Figure 10). During the thermal cycling, this volume retraction fluctuates between 5% (at -20 °C) and 8% (at -30 °C). The volume change that occurs at the cooling-freezing step could be related to the migration of the water initially inside the sponge cake matrix towards the macro-pores, where ice crystals are preferentially formed. When the sponge cake is warmed up to -20 °C, ice crystals sublimation can lead to dilatation particularly inside micropores where small crystals are more likely to sublimate. This results in a slight reduction of the volume retraction as can be seen in Figure 10. When the product is cooled down again to -30 °C, water diffuses through the matrix and evaporates inside the macropores but at a slower rate than during the first freezing step. Moreover gas entrapped in the closed pores may contract. Consequently, micropores may become smaller or disappear leading to the sample volume retraction. This mechanism is consistent with the results depicted in Figure 9 (b) that shows a decrease of the total number of pores during the whole experiment and an increase of the number of pores when the sponge cake is warmed up to -20 °C. This pore number increase is

accompanied by a decrease of the mean equivalent diameter of pores (Figure 9 (c)) meaning that these new pores are of small size (see section 3.2). To our knowledge, such results were not reported in the literature about sponge cake. Nevertheless, the shrinking phenomenon was extensively studied in bread crumb. Ribotta and Le Bail (2007) reported similar trend during freezing of bread. The authors argued that the retraction of bread crumb could be related to the dehydration of the matrix during freezing due to the removal of water from the protein-starch-water system in the form of ice. A bit later, Jiang et al. (2008) showed that cellular bread crumb (with pores) shrinks during freezing whereas degassed bread crumb expands. They also explained their results by the matrix dehydration following the formation of crystals inside the pores during freezing in the case of cellular bread crumb, while these crystals are formed inside the matrix in the case of degassed bread. More recently, this phenomenon was also noticed by Ben Aissa et al. (2010) while comparing cellular and degassed bread crumbs. Besides the hypothesis of the dehydration of the matrix, theses authors assumed the compression of the gas inside the pores to explain the shrinking behaviour of the cellular bread crumb. It is noteworthy that the levels of shrinkage reported in these works on bread are about 3% and therefore well below the results obtained in the case of this study with sponge cake. The difference could be related to the product composition, porosity or to freezing and frozen storage conditions. This remains to be investigated.

4. Conclusion

An original set-up, initially developed for snow, was used in order to characterize microstructural changes of a sponge cake sample during freezing and subsequent storage at fluctuating temperatures using X-ray tomog-

raphy. 3D images of the same sample were performed at different times during 6 days. An image processing based on Digital Volumetric Correlation (DVC) was implemented in order to segment the images and then to quantify porosity changes and ice crystal formation and growth. Several microstructural parameters (volume fraction of ice, air and matrix, number and equivalent diameter of pores and ice crystals, specific surface areas) were then computed from the 3D images. Overall, the obtained results of this first experiment have shown that:

1. during the freezing step, the sample was submitted to an important shrinkage of about 4-6%. During the seven warming-up/cooling cycles, this shrinkage was almost stable and oscillated between 5% and 8%. The macro-pores network of the sample is slightly affected by this shrinkage, whereas the small pores inside the matrix have disappeared.
2. during the thermal cycles, ice crystals mainly formed and enlarged at the macro-pore interface, whereas no crystal was found in the porous matrix. Thermal cycling was found to promote ice crystals growth due to the recrystallization phenomenon. Ice crystals size increased linearly with thermal cycling duration whereas their number tends towards a plateau.

In a near future, this experiment, which is long and complex, must be repeated in order to confirm the findings and to take into account the variability of food products. The obtained results open the way for future modeling to characterize the impact of freezing and frozen storage on the microstructure and quality of sponge cake. Moreover, the proposed methodology, which allows to study the microstructural changes of the same sample induced by complex thermal loadings, could be applied on other frozen porous products.

5. Acknowledgments

The authors would like to thank 3SR teams and CEN members for all their help and assistance during the tomography sessions. CNRM/CEN is part of the LabEx OSUG@2020 (Investissements d'Avenir, grant agreement ANR10 LABX56). 3SR Laboratory is part of the LabEx Tec21 (Investissements d'Avenir, grant agreement ANR11 269 LABX0030).

References

Baier-Schenk, A., Handschin, S., Von Schönau, M., Bittermann, A., Bächi, T., Conde-Petit, B., 2005. In situ observation of the freezing process in wheat dough by confocal laser scanning microscopy (clsm): Formation of ice and changes in the gluten network. Journal of Cereal Science 42, 255–260.

Bárcenas, M.E., Haros, M., Benedito, C., Rosell, C.M., 2003. Effect of freezing and frozen storage on the staling of part-baked bread. Food Research International 36, 863–869.

Bárcenas, M.E., Rosell, C.M., 2006. Effect of frozen storage time on the bread crumb and aging of par-baked bread. Food Chemistry 95, 438–445.

Ben Aissa, M.F., Monteau, J.Y., Perronnet, A., Roelens, G., Le Bail, A., 2010. Volume change of bread and bread crumb during cooling, chilling and freezing, and the impact of baking. Journal of Cereal Science 51, 115–119.

Buljac, A., Jailin, C., Mendoza, A., Neggers, J., Taillandier-Thomas, T., Bouterf, A., Smaniotto, B., Hild, F., Roux, S., 2018. Digital volume

782 correlation: review of progress and challenges. Experimental Mechanics
783 58, 661–708.

784 Calonne, N., Flin, F., Lesaffre, B., Dufour, A., Roulle, J., Puglièse, P.,
785 Philip, A., Lahoucine, F., Geindreau, C., Panel, J.M., et al., 2015.
786 CellDyM: a room temperature operating cryogenic cell for the dynamic
787 monitoring of snow metamorphism by time-lapse x-ray microtomography.
788 Geophysical Research Letters 42, 3911–3918.

789 Chen, G., Jansson, H., Lustrup, K.F., Swenson, J., 2012. Formation and
790 distribution of ice upon freezing of different formulations of wheat bread.
791 Journal of Cereal Science 55, 279–284.

792 Chen, G., Öhgren, C., Langton, M., Lustrup, K.F., Nydén, M., Swenson, J.,
793 2013. Impact of long-term frozen storage on the dynamics of water and
794 ice in wheat bread. Journal of cereal science 57, 120–124.

795 Cook, K., Hartel, R., 2010. Mechanisms of ice crystallization in ice cream
796 production. Comprehensive Reviews in Food Science and Food Safety 9,
797 213 – 222. doi:10.1111/j.1541-4337.2009.00101.x.

798 Díaz-Ramírez, M., Calderón-Domínguez, G., Salgado-Cruz, M.d.l.P.,
799 Chanona-Pérez, J.J., Andraca-Adame, J.A., Ribotta, P.D., 2016. Sponge
800 cake microstructure, starch retrogradation and quality changes during
801 frozen storage. International Journal of Food Science & Technology 51,
802 1744–1753.

803 Eckardt, J., Öhgren, C., Alp, A., Ekman, S., Åström, A., Chen, G., Swenson,
804 J., Johansson, D., Langton, M., 2013. Long-term frozen storage of wheat

bread and dough–effect of time, temperature and fibre on sensory quality, microstructure and state of water. Journal of Cereal Science 57, 125–133.

Fennema, O., 1973. Nature of freezing process. Marcel Dekker,, New York. pp. 151–222.

Glover, G., Pelc, N., 1980. Nonlinear partial volume artifacts in x-ray computed tomography. Medical physics 7, 238–248.

Guo, E., Kazantsev, D., Mo, J., Bent, J., Van Dalen, G., Schuetz, P., Rockett, P., StJohn, D., Lee, P.D., 2018. Revealing the microstructural stability of a three-phase soft solid (ice cream) by 4d synchrotron x-ray tomography. Journal of food engineering 237, 204–214.

Gómez, M., Ruiz, E., Oliete, B., 2011. Effect of batter freezing conditions and resting time on cake quality. LWT - Food Science and Technology 44, 911–916.

Hamdami, N., Monteau, J.Y., Le Bail, A., 2004. Thermophysical properties evolution of french partly baked bread during freezing. Food Research International 37, 703–713.

Hartel, R.W., 1998. Mechanisms and kinetics of recrystallization in ice cream. Springer US, Boston, MA. pp. 287–319.

Hild, F., Fanget, A., Adrien, J., Maire, E., Roux, S., 2011. Three-dimensional analysis of a tensile test on a propellant with digital volume correlation. Archives of Mechanics Vol. 63, nr 5-6, 459–478.

Jiang, Z., Le Bail, A., Wu, A., 2008. Effect of the thermostable xylanase b (xynb) from thermotoga maritima on the quality of frozen partially baked bread. Journal of Cereal Science 47, 172–179.

Karaoğlu, M.M., Kotancilar, H.G., Gerçekaslan, K.E., 2008. The effect of par-baking and frozen storage time on the quality of cup cake. International Journal of Food Science & Technology 43, 1778–1785.

Kontogiorgos, V., Goff, H.D., 2006. Calorimetric and microstructural investigation of frozen hydrated gluten. Food Biophysics 1, 202–215.

Kontogiorgos, V., Goff, H.D., Kasapis, S., 2008. Effect of aging and ice-structuring proteins on the physical properties of frozen flour–water mixtures. Food Hydrocolloids 22, 1135–1147.

Le-Bail, A., Tzia, C., Giannou, V., 2011. Quality and Safety of Frozen Bakery Products, In: Sun, DW (eds) Handbook of Frozen Food Processing and Packaging, Boca Raton, Florida: CRC Press. pp. 501–528.

Legland, D., Arganda-Carreras, I., Andrey, P., 2016. Morpholibj: integrated library and plugins for mathematical morphology with imagej. Bioinformatics 32, 3532–3534.

Lenoir, N., Bornert, M., Desrues, J., Bésuelle, P., Viggiani, G., 2007. Volumetric digital image correlation applied to x-ray microtomography images from triaxial compression tests on argillaceous rock. Strain 43, 193–205.

Leplay, P., Rethore, J., Meille, S., Baietto, M.C., Adrien, J., Chevalier, J., Maire, E., 2013. Three-dimensional analysis of an in situ double-torsion test by x-ray computed tomography and digital volume correlation. Experimental Mechanics 53, 1265–1275.

Limodin, N., Réthoré, J., Buffière, J.Y., Hild, F., Ludwig, W., Rannou, J., Roux, S., 2011. 3d x-ray microtomography volume correlation to study fatigue crack growth. Advanced Engineering Materials 13, 186–193.

Lucas, T., Le Ray, D., Davenel, A., 2005a. Chilling and freezing of part-baked bread. part i: An mri signal analysis. Journal of food engineering 70, 139–149.

Lucas, T., Quellec, S., Le Bail, A., Davenel, A., 2005b. Chilling and freezing of part-baked bread. part ii: Experimental assessment of water phase changes and structure collapse. Journal of Food Engineering 70, 151–164.

Mandala, I., Kapetanakou, A., Kostaropoulos, A., 2008. Physical properties of breads containing hydrocolloids stored at low temperature: Ii-effect of freezing. Food Hydrocolloids 22, 1443–1451.

Mandala, I., Polaki, A., Yanniotis, S., 2009. Influence of frozen storage on bread enriched with different ingredients. Journal of Food Engineering 92, 137–145.

Masselot, V., Bosc, V., Benkhelifa, H., 2021. Analyzing the microstructure of a fresh sorbet with x-ray micro-computed tomography: Sampling, acquisition, and image processing. Journal of Food Engineering 292, 13–21.

Mulot, V., Ndoye, F.T., Benkhelifa, H., Pathier, D., Flick, D., 2019. Investigating the effect of freezing operating conditions on microstructure of frozen minced beef using an innovative x-ray micro-computed tomography method. Journal of Food Engineering 262, 13–21.

Ndoye, F., Alvarez, G., 2014. Characterization of ice recrystallization in ice cream during storage using the focused beam reflectance measurement. Journal of Food Engineering 148. doi:10.1016/j.jfoodeng.2014.09.014.

Owen, R.F., Van Duyne, F.O., 1950. Comparison of the quality of freshly

baked cakes, thawed frozen baked cakes, and cakes prepared from batters which had been frozen. Journal of Food Science 15, 169–178.

Pham, Q.T., 2006. Modelling heat and mass transfer in frozen foods: a review. International Journal of Refrigeration 29, 876–888. Issue with Special Emphasis on Data and Models on Food Refrigeration.

Pierron, F., McDonald, S., Hollis, D., Fu, J., Withers, P., Alderson, A., 2013. Comparison of the mechanical behaviour of standard and auxetic foams by x-ray computed tomography and digital volume correlation. Strain 49, 467–482.

Ribotta, P.D., Le Bail, A., 2007. Thermo-physical assessment of bread during staling. LWT - Food Science and Technology 40, 879–884.

Roux, S., Hild, F., Viot, P., Bernard, D., 2008. Three-dimensional image correlation from x-ray computed tomography of solid foam. Composites Part A: Applied science and manufacturing 39, 1253–1265.

Seghir, R., Witz, J.F., Courdert, S., 2014. Yadics-digital image correlation 2/3d software. URL: `http://www.yadics.univ-lille1.fr`.

Vicent, V., Ndoye, F.T., Verboven, P., Nicolaï, B., Alvarez, G., 2019. Effect of dynamic storage temperatures on the microstructure of frozen carrot imaged using x-ray micro-ct. Journal of Food Engineering 246, 232–241.

Vicent, V., Verboven, P., Ndoye, F.T., Alvarez, G., Nicolaï, B., 2017. A new method developed to characterize the 3d microstructure of frozen apple using x-ray micro-ct. Journal of Food Engineering 212, 154–164.

Wang, L., Limodin, N., El Bartali, A., Witz, J.F., Seghir, R., Buffiere, J.Y., Charkaluk, E., 2016. Influence of pores on crack initiation in monotonic

tensile and cyclic loadings in lost foam casting a319 alloy by using 3d in-situ analysis. Materials Science and Engineering: A 673, 362–372.

van Westen, T., Groot, R., 2018. The effect of temperature cycling on ostwald ripening. Crystal Growth Design 18. doi:10.1021/acs.cgd.8b00267.

Zaritzky, N., 2010. 20 - chemical and physical deterioration of frozen foods, in: Skibsted, L.H., Risbo, J., Andersen, M.L. (Eds.), Chemical Deterioration and Physical Instability of Food and Beverages. Woodhead Publishing. Woodhead Publishing Series in Food Science, Technology and Nutrition, pp. 561–607.

Zariztky, N., 2008. Frozen Storage, in: Evans, J.A. (Ed) Frozen Food Science and Technology. Blackwell Publishing Ltd. pp. 224–247.

List of Figures

1 Typical ice melting endotherm obtained upon the thawing of frozen sponge cake with a heating rate of 5 °C/min. 40

2 (a) Photographs of the experiment, overview of the CellDyM cryogenic cell installed in the tomograph cabin (RX Solutions, France) before the experiment, and (b) photograph of the 10 mm high sample before its installation inside CellDyM. . . . 41

3 Freezing and temperature cycles. The dots show the realised scans, note that they were made at least 30 minutes after a temperature change for thermalisation purposes. 42

4 Image processing procedure. 43

5 (a) Vertical slice of the 3D grey level image for scan S36. (b) Zoomed region of the image, which reveals the ice crystals within the sample. (c) Grey levels histogram of the slice that highlights the difficulty to segment the three phases by direct grey level thresholding. (d) Vertical slice of the residue 3D image for scan S36. (e) Zoomed region of the image showing the ice crystals in black. (f) Residue histogram with its Gaussian model for noise. (g) The result label image, and (h) its associated zoomed region. 44

6 Schematic representation of the sponge cake phases and interfaces. 45

7 Cryo-SEM image of a fractured frozen sponge cake. 45

8 Vertical slices of some 3D images showing the evolution of the matrix microstructure and the growth of the ice crystals during the experiment. 46

9 Evolution during the experiment of: (a) the distribution of the equivalent diameters of the pores $d_{\mathrm{eq}}^{\mathrm{pore}}$, the class width is 0.1 mm, each scan in represented by a color, (b) the number of pores inside the sample N^{pore}, and (c) the mean equivalent diameter of these pores $\langle d_{\mathrm{eq}} \rangle$. The orange shaded areas correspond to the estimated error. 47

10 Evolution of the sample volume V_{sample}/V_0 during the experiment. 47

11 Vertical profiles of the 3 phases' volume fractions during the experiment: (a) matrix (cake) volume fraction V_{matrix}/V_0, (b) air volume fraction (porosity) V_{air}/V_0, and (c) ice volume fraction V_{ice}/V_0. 48

12 Evolution during the experiment of the (a) matrix volume fraction V_{matrix}/V_0, (b) air volume fraction (porosity) V_{air}/V_0, and (c) ice volume fraction V_{ice}/V_0. 48

13 3D rendering of matrix (yellow) and ice crystals (blue). The length of the edges of the bounding box is 1 mm. 49

14 Evolution of the granulometry of the ice crystals during the experiment: (a) equivalent diameter distribution (class width: 10 µm), (b) number of ice crystals, and (c) mean ice crystal volume v^{ice}. 50

15 Evolution during the experiment of the specific surface areas between the 3 phases: air, matrix and ice, SSA(interface) = $S(\mathrm{interface})/V_0$. 50

16 Physics of the sponge cake during its freezing and storage. . . 51

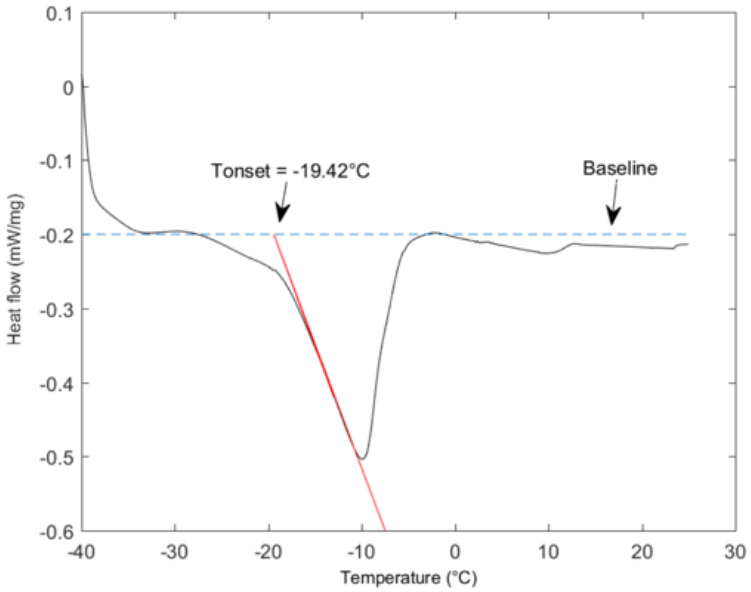

Figure 1: Typical ice melting endotherm obtained upon the thawing of frozen sponge cake with a heating rate of 5 °C/min.

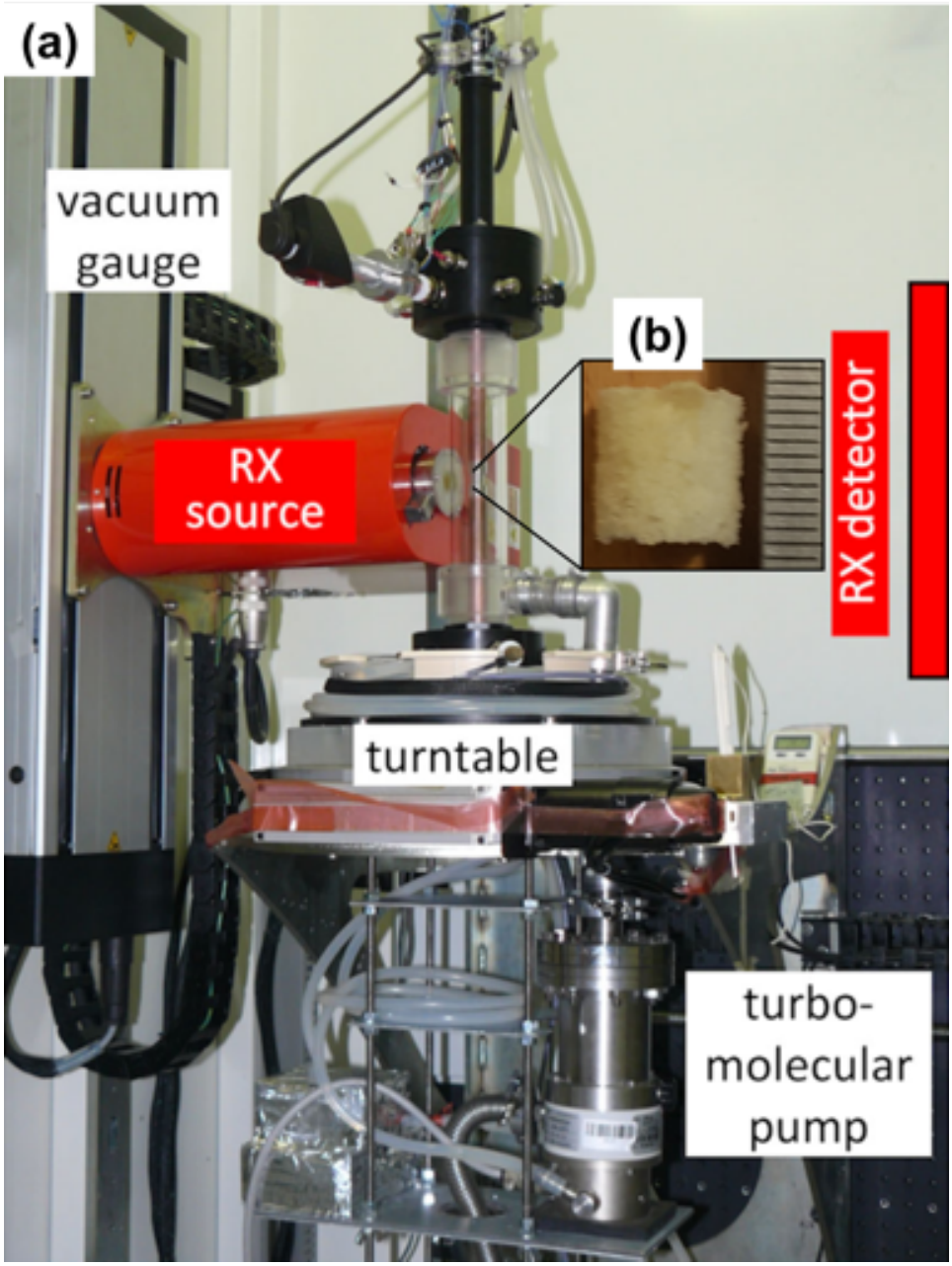

Figure 2: (a) Photographs of the experiment, overview of the CellDyM cryogenic cell installed in the tomograph cabin (RX Solutions, France) before the experiment, and (b) photograph of the 10 mm high sample before its installation inside CellDyM.

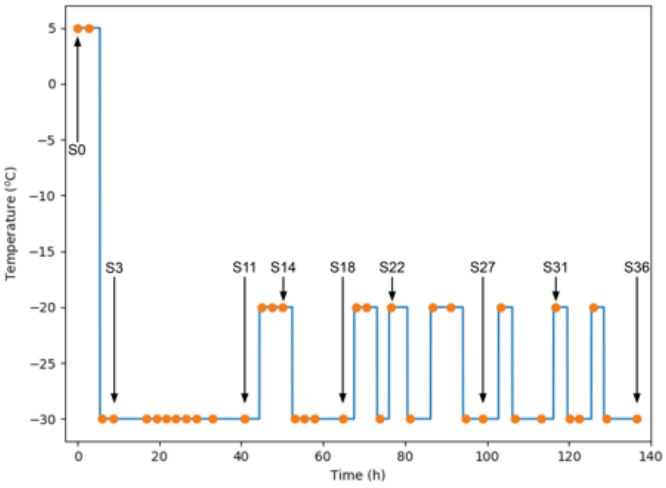

Figure 3: Freezing and temperature cycles. The dots show the realised scans, note that they were made at least 30 minutes after a temperature change for thermalisation purposes.

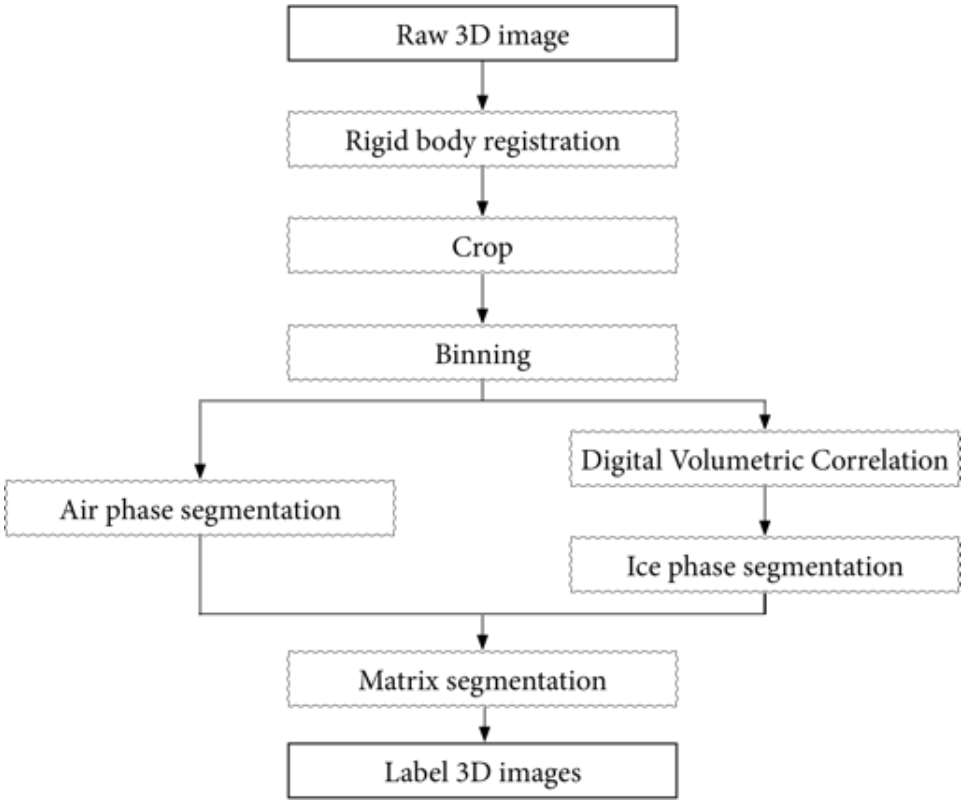

Figure 4: Image processing procedure.

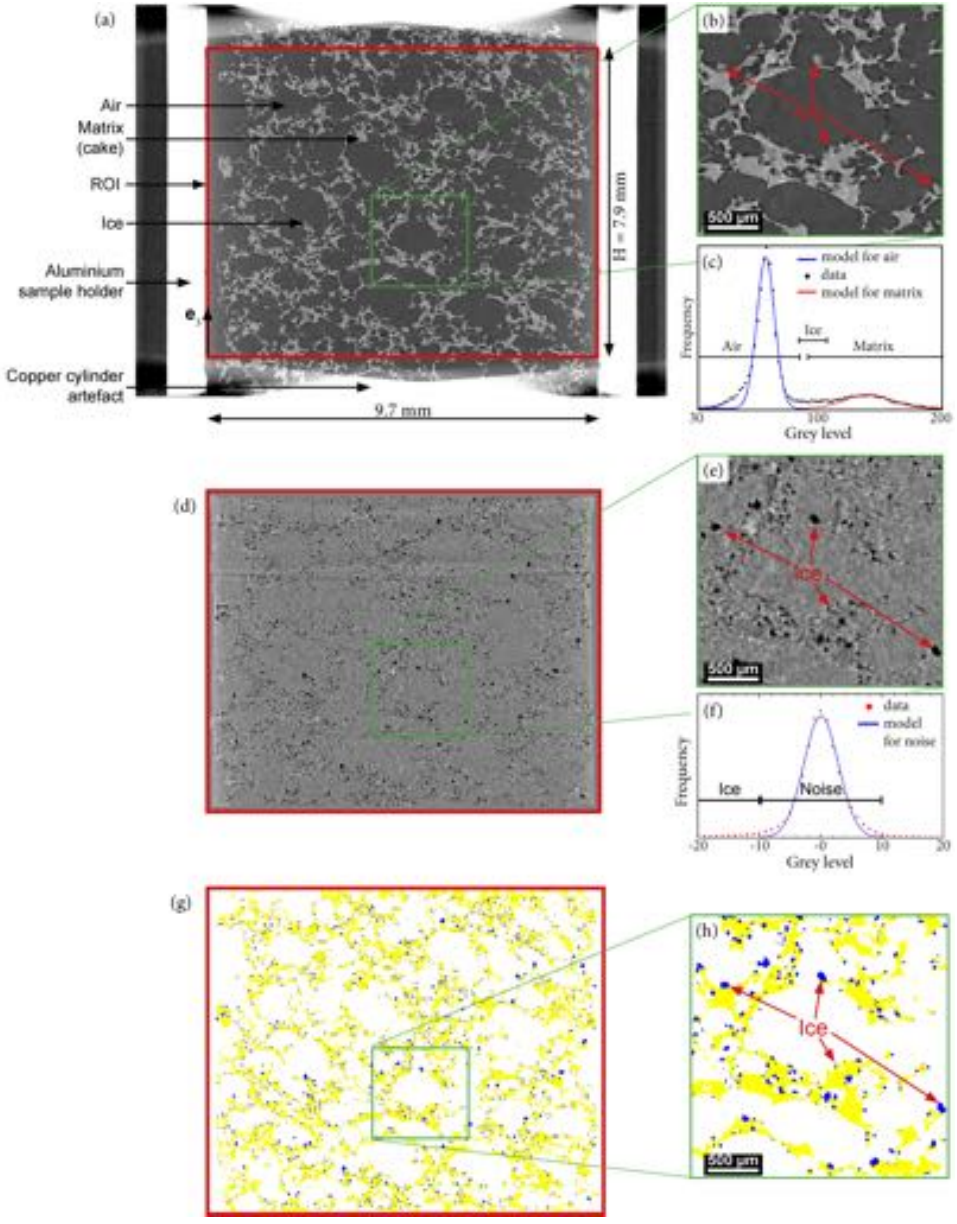

Figure 5: (a) Vertical slice of the 3D grey level image for scan S36. (b) Zoomed region of the image, which reveals the ice crystals within the sample. (c) Grey levels histogram of the slice that highlights the difficulty to segment the three phases by direct grey level thresholding. (d) Vertical slice of the residue 3D image for scan S36. (e) Zoomed region of the image showing the ice crystals in black. (f) Residue histogram with its Gaussian model for noise. (g) The result label image, and (h) its associated zoomed region.

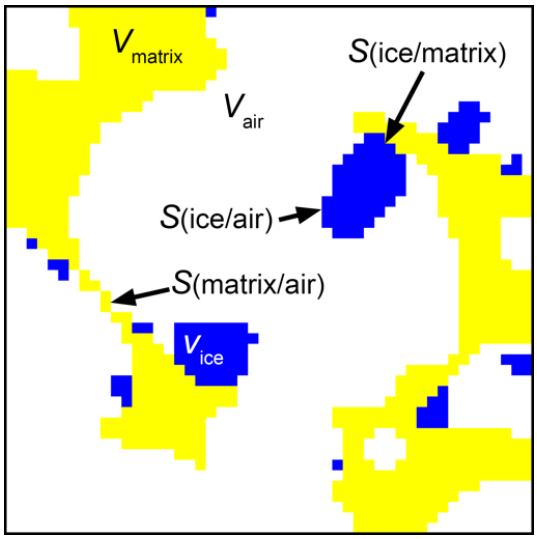

Figure 6: Schematic representation of the sponge cake phases and interfaces.

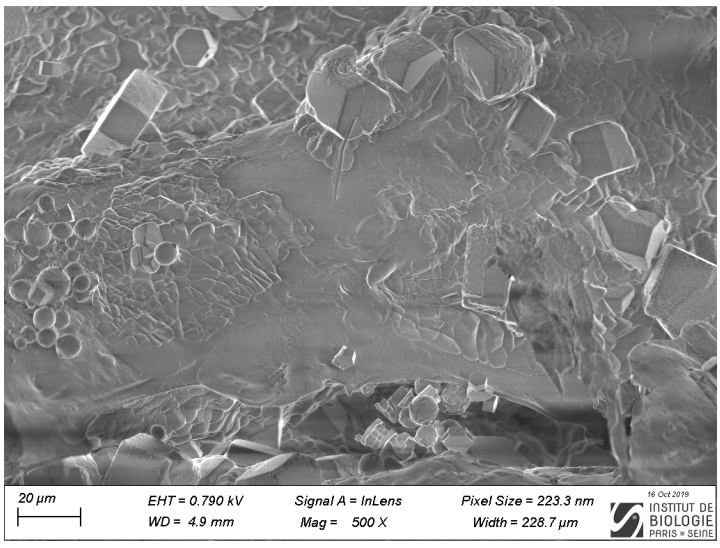

Figure 7: Cryo-SEM image of a fractured frozen sponge cake.

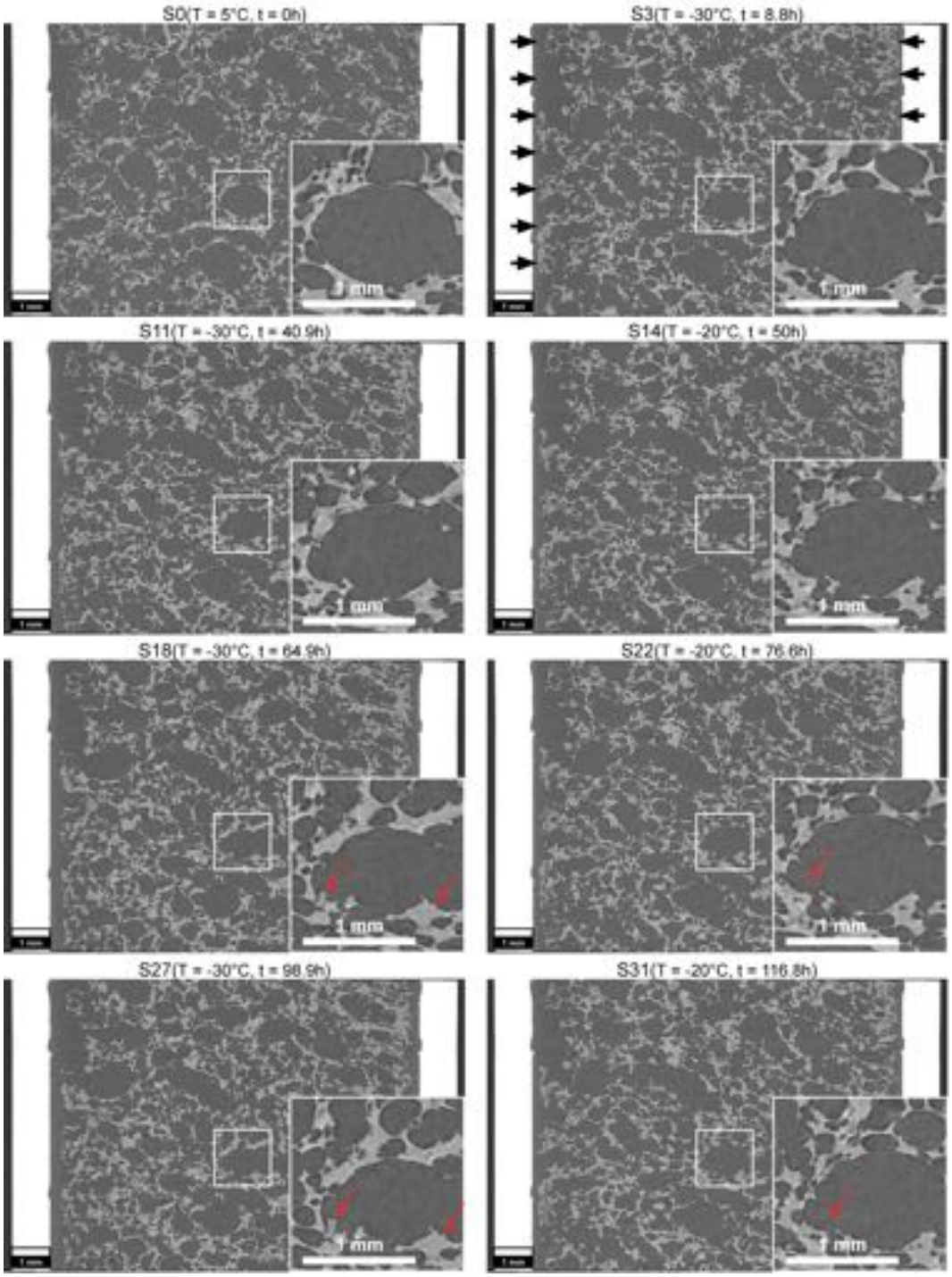

Figure 8: Vertical slices of some 3D images showing the evolution of the matrix microstructure and the growth of the ice crystals during the experiment.

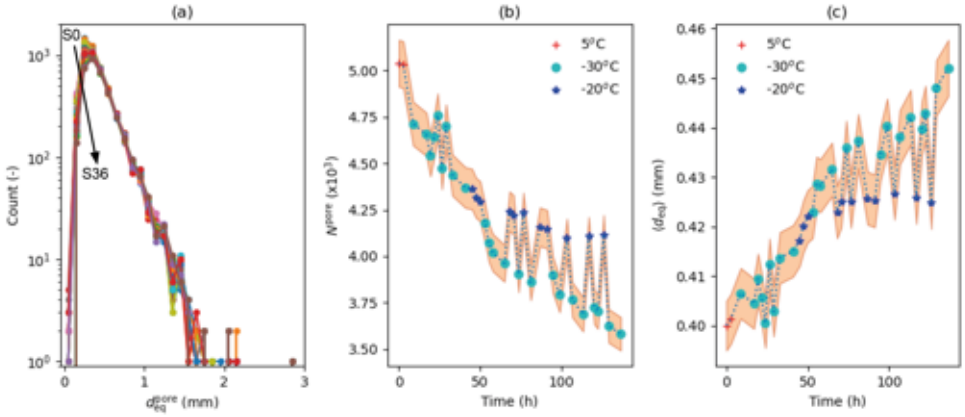

Figure 9: Evolution during the experiment of: (a) the distribution of the equivalent diameters of the pores $d_{\text{eq}}^{\text{pore}}$, the class width is 0.1 mm, each scan in represented by a color, (b) the number of pores inside the sample N^{pore}, and (c) the mean equivalent diameter of these pores $\langle d_{\text{eq}} \rangle$. The orange shaded areas correspond to the estimated error.

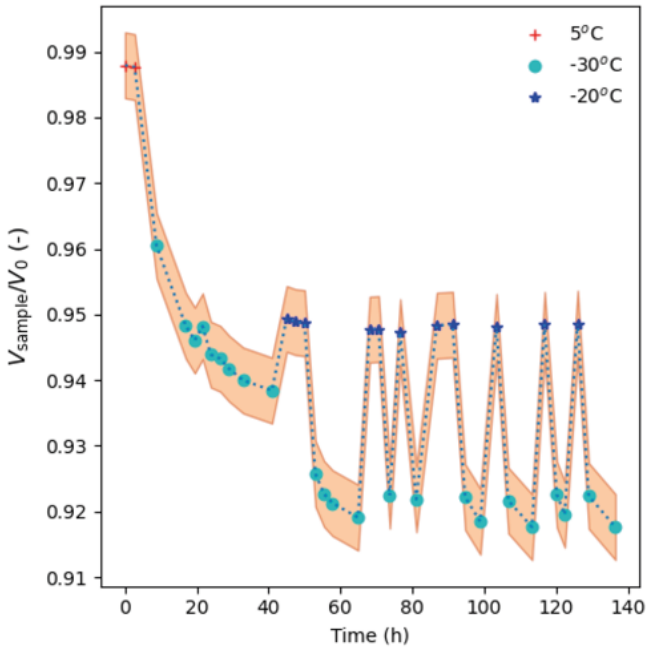

Figure 10: Evolution of the sample volume V_{sample}/V_0 during the experiment.

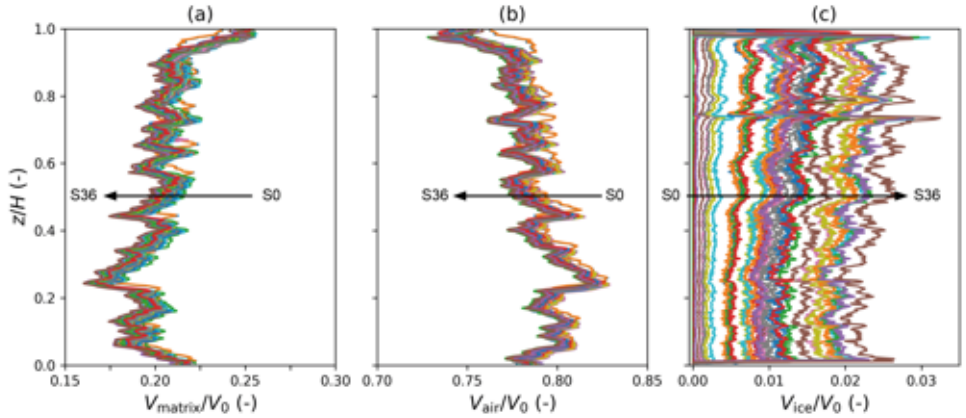

Figure 11: Vertical profiles of the 3 phases' volume fractions during the experiment: (a) matrix (cake) volume fraction V_{matrix}/V_0, (b) air volume fraction (porosity) V_{air}/V_0, and (c) ice volume fraction V_{ice}/V_0.

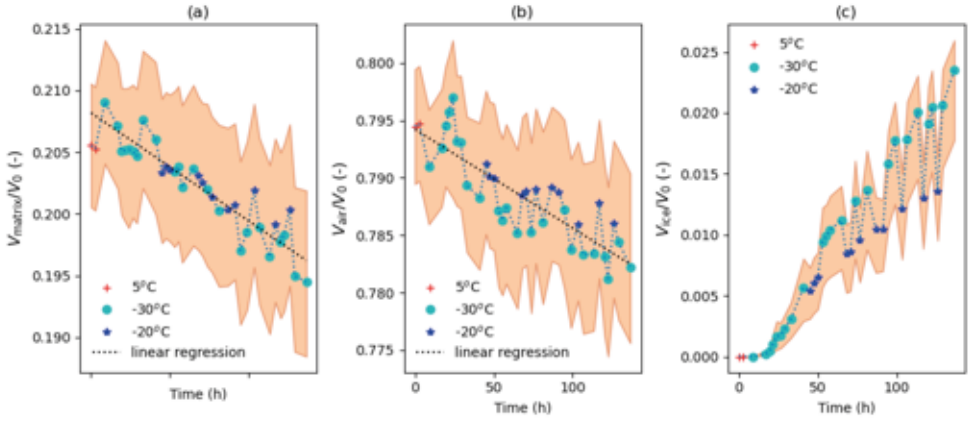

Figure 12: Evolution during the experiment of the (a) matrix volume fraction V_{matrix}/V_0, (b) air volume fraction (porosity) V_{air}/V_0, and (c) ice volume fraction V_{ice}/V_0.

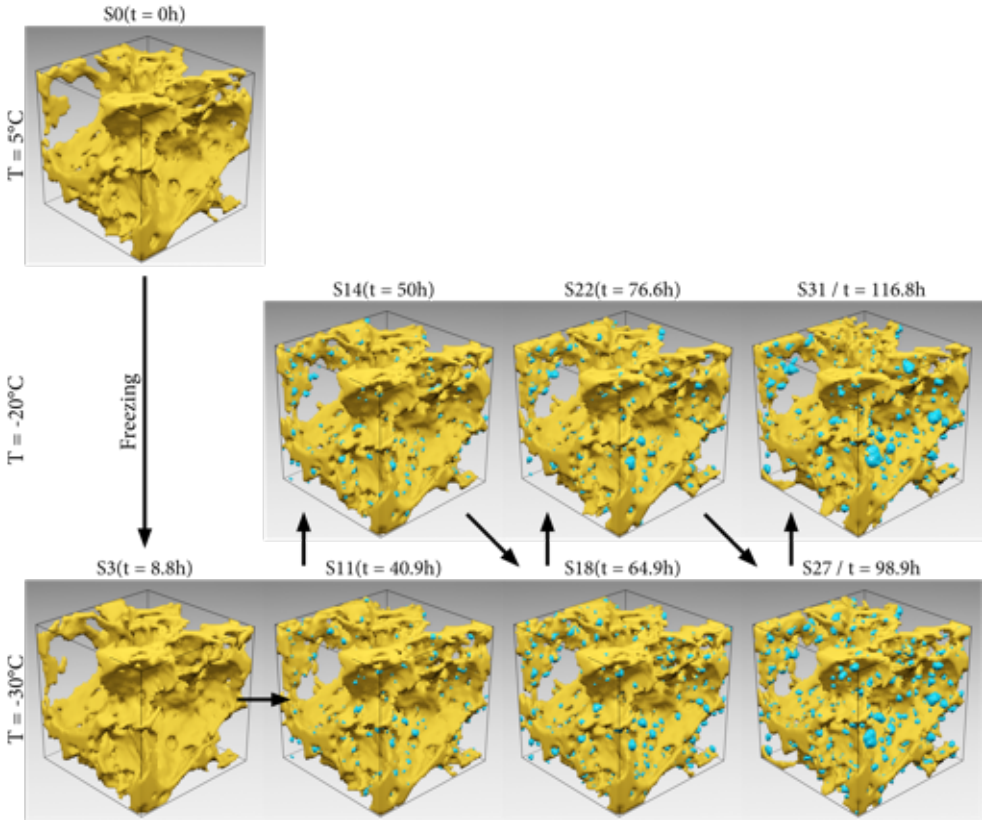

Figure 13: 3D rendering of matrix (yellow) and ice crystals (blue). The length of the edges of the bounding box is 1 mm.

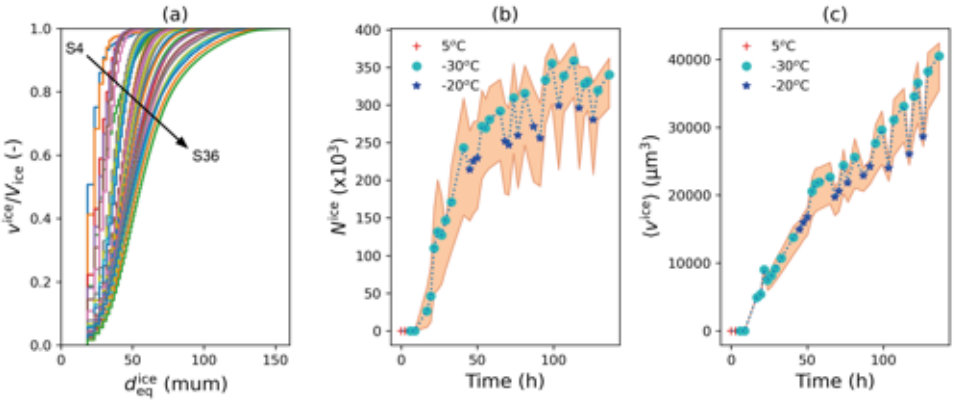

Figure 14: Evolution of the granulometry of the ice crystals during the experiment: (a) equivalent diameter distribution (class width: 10 µm), (b) number of ice crystals, and (c) mean ice crystal volume v^{ice}.

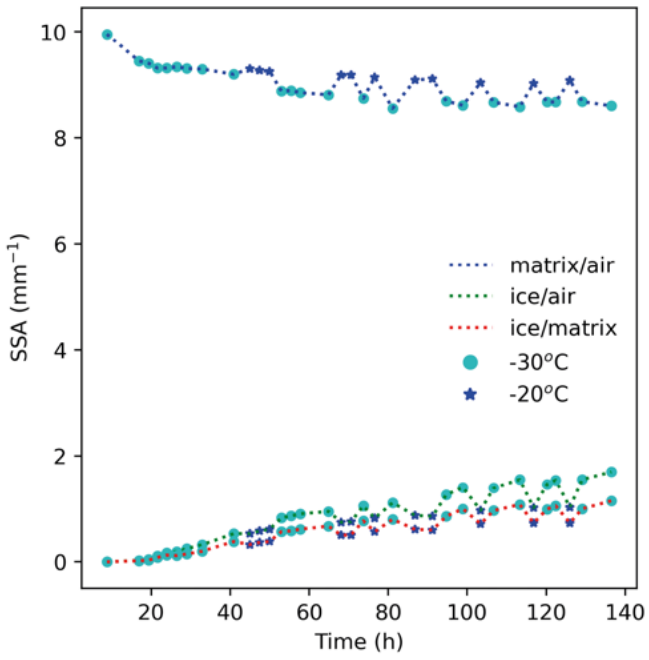

Figure 15: Evolution during the experiment of the specific surface areas between the 3 phases: air, matrix and ice, SSA(interface) = S(interface)/V_0.

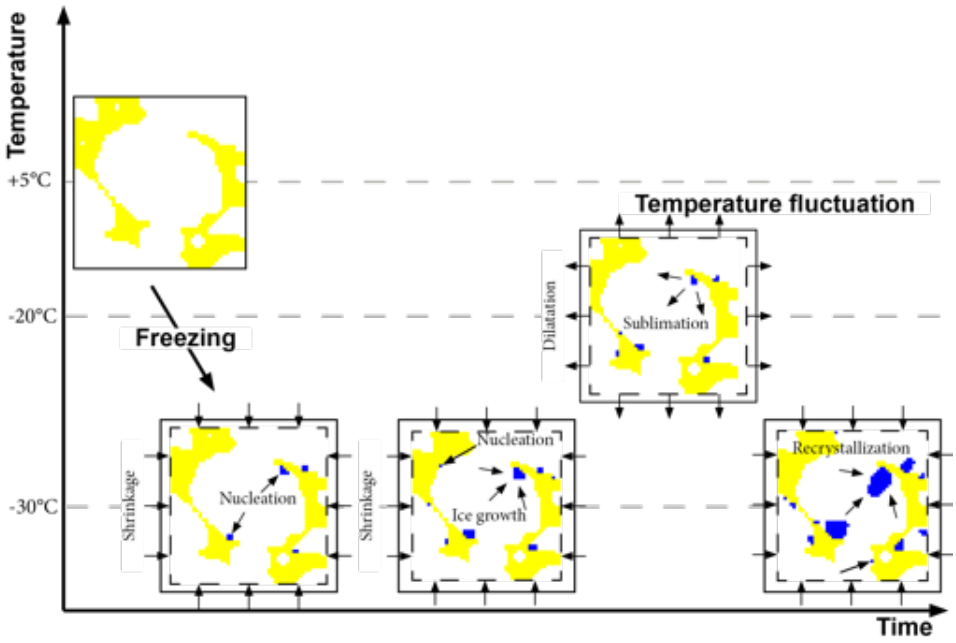

Figure 16: Physics of the sponge cake during its freezing and storage.

CRediT author statement

Manuscript title: "X-ray microtomography of ice crystal formation and growth in a sponge cake during its freezing and storage"

Author's name	Contribution
Pierre LATIL	Conceptualization, Methodology, Investigation, Validation, Formal analysis, , Writing - Original Draft Preparation, writing, review and editing, Visualization, Software
Amira ZENNOUNE	Conceptualization, Methodology, Investigation, Validation, Formal analysis, Writing - Original Draft Preparation, writing, review and editing, ,
Fatou-Toutie NDOYE	Conceptualization, , Validation, writing, review and editing , Project administration, Funding acquisition
Frederic FLIN	Conceptualization, Methodology, Investigation, Validation Formal analysis, Resources, , writing, review and editing, Software
Hayat BENKHELIFA	Conceptualization , writing, review and editing, Supervision, Project administration, Funding acquisition
Christian GEINDREAU	Conceptualization, writing, review and editing, Supervision, Project administration, Funding acquisition

Conflict of Interest and Authorship Conformation Statement

Manuscript title: "X-ray microtomography of ice crystal formation and growth in a sponge cake during its freezing and storage"

Dear Editor,

We confirm that this manuscript has not been published and is not under consideration for publication elsewhere. All co-authors have seen and agree with the contents of the manuscript, and we have no conflicts of interest to disclose.

Author's name	Affiliation
Pierre LATIL	Centre d'étude de la neige Grenoble France
Amira ZENNOUNE	INRAE, FRISE , France AgroParisTech, France
Fatou-Toutie NDOYE	INRAE, FRISE France
Frederic FLIN	Centre d'étude de la neige Grenoble France
Hayat BENKHELIFA	INRAE, FRISE , France AgroParisTech, France
Christian GEINDREAU	3SR Grenoble, France